Electronic Supplementary Material

Effect of tandem-type stabilization of Nb_2CT_x MXene on their colloidal and cytotoxic properties

M. Jakubczak (✉)[1], A. Wojciechowska[2], J. Mitrzak[2], A. Szuplewska[3], M. Chudy[3], A. Wójcik[4], D. Moszczyńska[2], K. Prenger[5], M. Naguib[5,6], and A. M. Jastrzębska[1]

1 Faculty of Mechatronics, Warsaw University of Technology, św. Andrzeja Boboli 8, 02-525 Warsaw, Poland
2 Faculty of Materials Science and Engineering, Warsaw University of Technology, Wołoska 141, 02-507 Warsaw, Poland
3 Faculty of Chemistry, Noakowskiego 3, 00-664 Warsaw, Poland
4 Polish Academy of Sciences, Institute of Metallurgy and Materials Science, W. Reymonta 25, 30-059 Cracow, Poland
5 Department of Physics and Engineering Physics, Tulane University, New Orleans, LA 70118, USA
6 Department of Chemistry, Tulane University, New Orleans, LA 70118, USA

E-mail: michal.jakubczak.dokt@pw.edu.pl

To complement the structural and morphological analyses the particle size and shape distribution of the Nb_2AlC MAX phase powder was examined using dynamic particle shape analysis. Measurements were carried out using Sentinel Pro (Micromeritics Instrument Corporation, Norcross, GA, USA) equipped with a peristaltic pump and a stroboscopic camera. This dynamic fluid-flow setup enables a three-dimensional, randomly oriented, and real-time assessment of particles in motion, providing high-resolution particle images for subsequent post-measurement processing. The technique allows for the extraction of multiple shape-related parameters, including equivalent circular area diameter (ECAD), circularity, Feret length, and Feret width, which were employed to quantify both the size distribution and morphological uniformity of the ground Nb_2AlC MAX phase. Obtained results were presented in Fig. S1.

Dynamic particle shape analysis was employed to provide quantitative characterization of the particle size and shape distribution of the Nb_2AlC MAX phase powder (Fig. S1). The equivalent circular area diameter (ECAD) distribution (Fig. S1(a)) revealed that the majority of particles possessed submicron dimensions (< 1 μm), with an additional pronounced peak at approximately 12.7 μm, indicating the presence of larger grains. The circularity analysis (Fig. S1(b)) demonstrated that most particles exhibited values around 0.33, suggesting irregular morphologies, although a significant fraction of grains reached circularity values of ~0.68, consistent with more equiaxed particles. The Feret length distribution (Fig. S1(c)) showed two dominant populations, with a high number of particles below 1 μm and a secondary maximum around 16 μm. A similar bimodal trend was observed in the Feret width distribution (Fig. S1(d)), with maxima below 1 μm and at ~12.7 μm. Importantly, the ratio of Feret length to Feret width for the majority of particles approached unity, indicating that most grains are nearly equiaxed and close to spherical in shape. Representative particle images obtained during analysis (Fig. S1(e)) further confirmed this observation, showing individual Nb_2AlC grains with morphologies consistent with near-spherical particles. Taken together, these results confirm that the ground Nb_2AlC MAX phase powder consists predominantly of uniformly distributed, equiaxed grains with a submicron fraction and a secondary population in the 12–16 μm range, in agreement with the morphology typically reported for MAX phases [S1–S3].

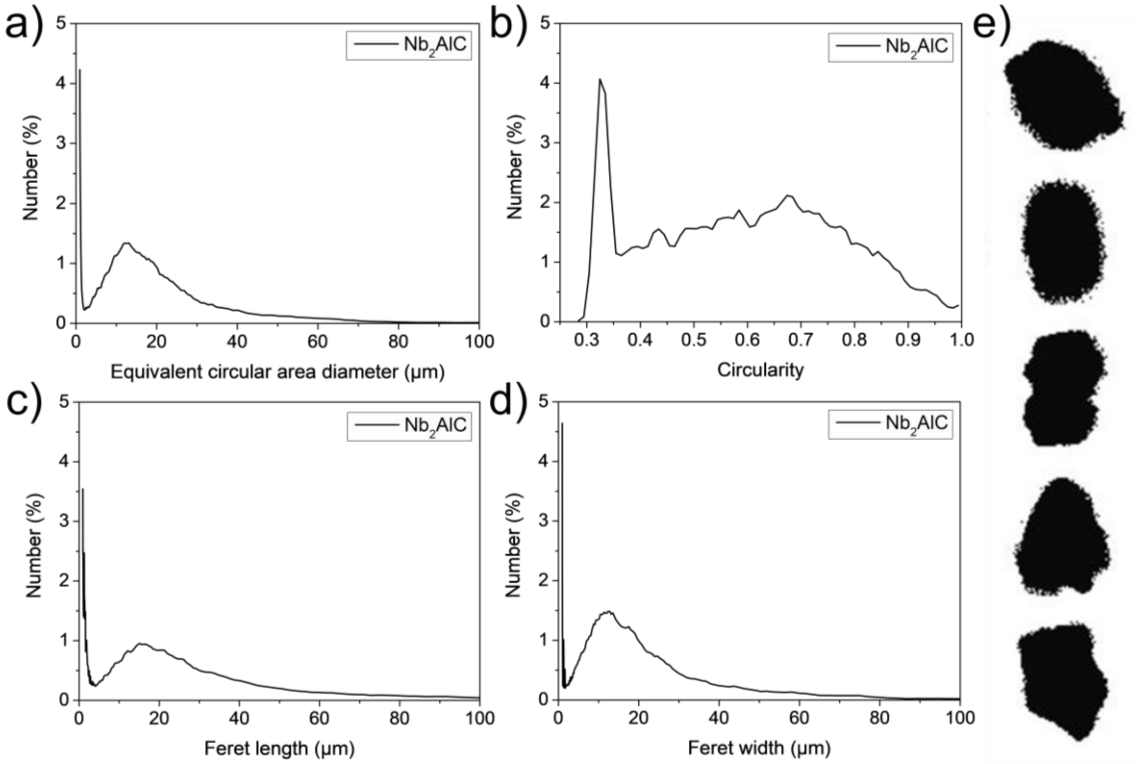

Fig. S1 Results of the dynamic particle shape analysis performed for the Nb_2AlC MAX phase and considering parameters such as **(a)** equivalent circular area diameter, **(b)** circularity, **(c)** Feret length and **(d)** Feret width, with **(e)** representative particle images obtained during analysis.

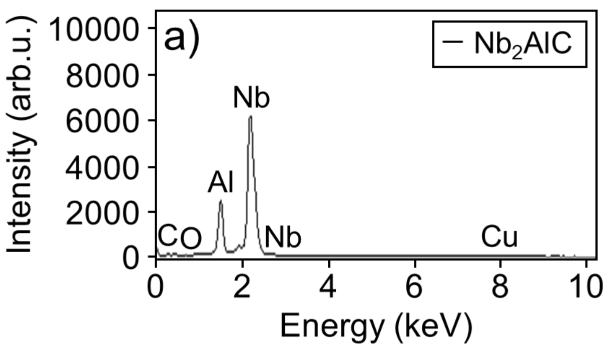

b)

Element	Wt.%	At.%
C	9.97 ± 0.64	38.95 ± 2.49
O	1.00 ± 0.15	2.93 ± 0.43
Al	10.39 ± 0.10	18.07 ± 0.18
Cu	1.43 ± 0.35	1.06 ± 0.26
Nb	77.21 ± 0.53	39.00 ± 0.27

Fig. S2 (a) EDS spectrum obtained for the parental Nb_2AlC MAX phase along with **(b)** corresponding quantitative summary of the analysis.

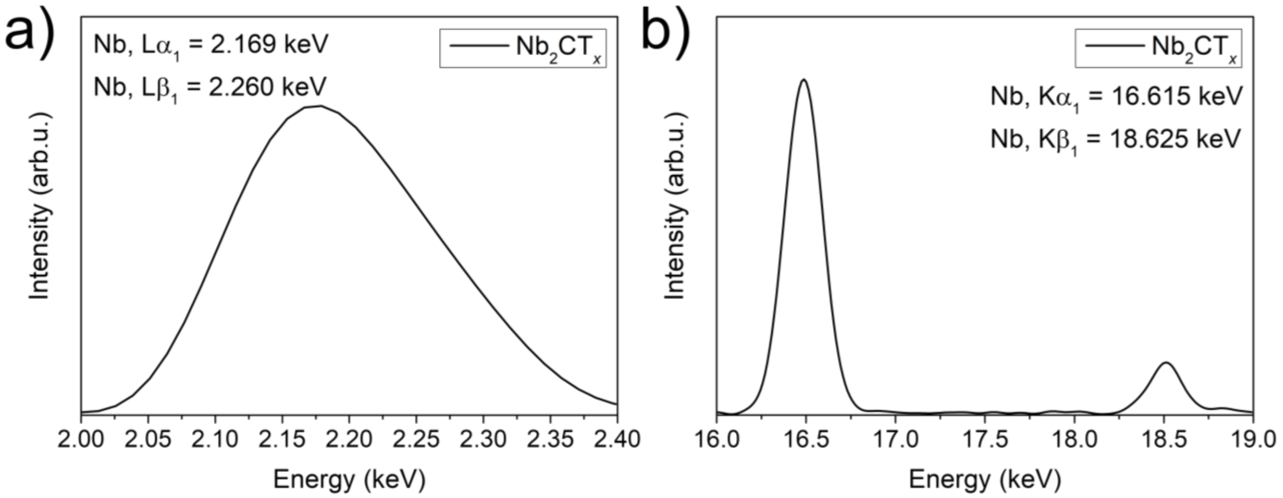

Fig. S3 XRF studies showing the presence of Nb in SL Nb_2CT_x MXene. The analysis focused on the $L\alpha_1$ and $L\beta_1$ (2.169 and 2.260 keV, respectively), as well as the $K\alpha_1$ and $K\beta_1$ (16.615 and 18.625 keV, respectively) emissions.

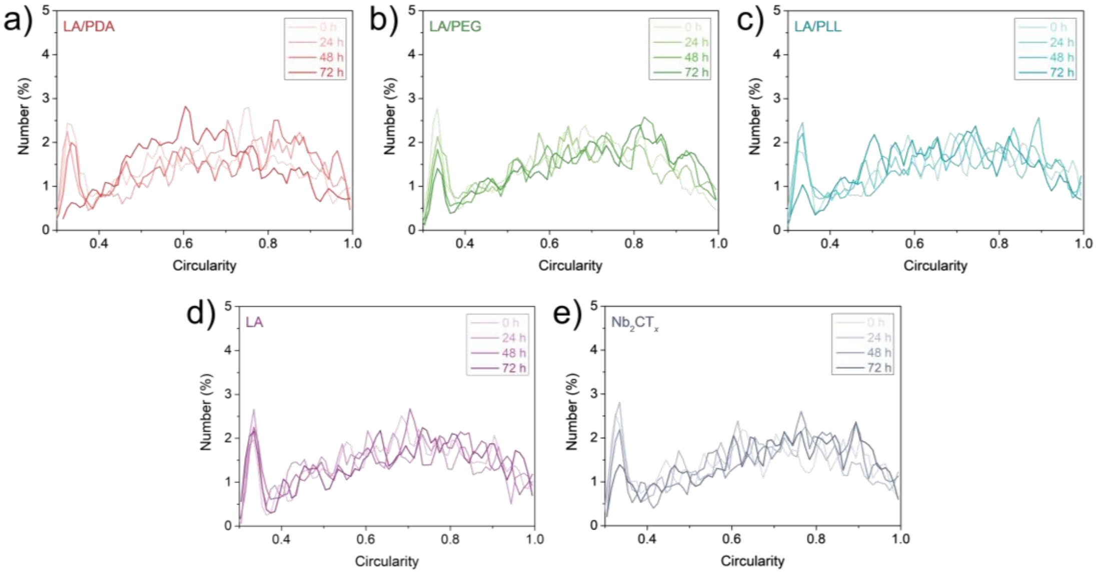

Fig. S4 Results of circularity coefficient measurements performed for the SL Nb_2CT_x MXene, stabilized with **(a)** LA/PDA, **(b)** LA/PEG, **(c)** LA/PLL, and **(d)** LA, as well as for **(e)** unmodified SL Nb_2CT_x MXene over time in DMEM solution.

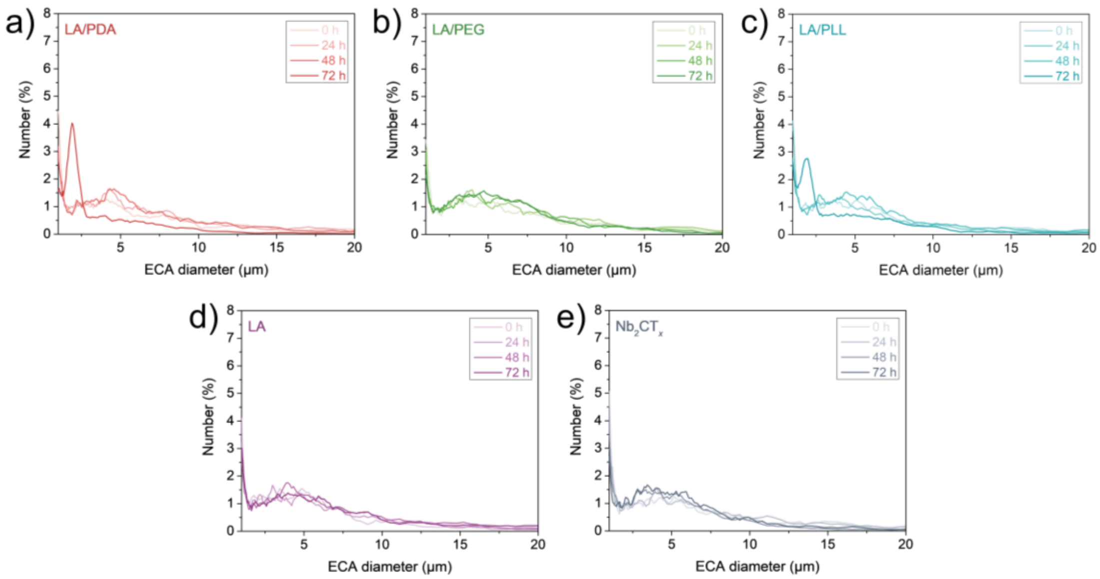

Fig. S5 Results of equivalent circular area diameter performed for the SL Nb_2CT_x MXene, stabilized with **(a)** LA/PDA, **(b)** LA/PEG, **(c)** LA/PLL, and **(d)** LA, as well as for **(e)** unmodified SL Nb_2CT_x MXene over time in the DMEM solution.

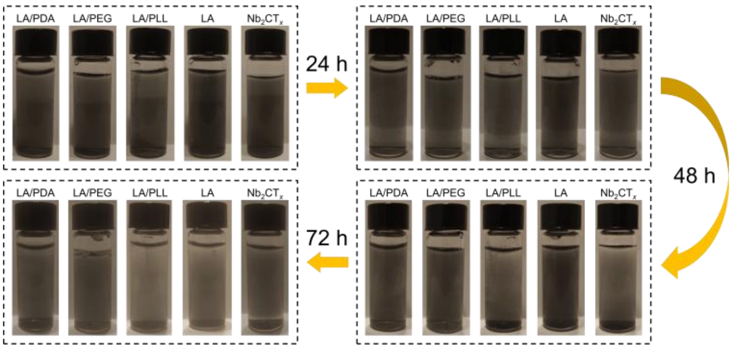

Fig. S6 Photographs of the SL Nb_2CT_x MXene, stabilized with LA/PDA, LA/PEG, LA/PLL, and LA, as well as for unmodified SL Nb_2CT_x MXene over time in the DMEM solution at different time points (0, 24, 48, and 72 h). The images visually illustrate differences in colloidal stability over time, confirming that surface functionalization with LA/PDA, LA/PEG, and LA/PLL alters dispersion stability compared to unmodified SL Nb_2CT_x MXene and LA-only samples.

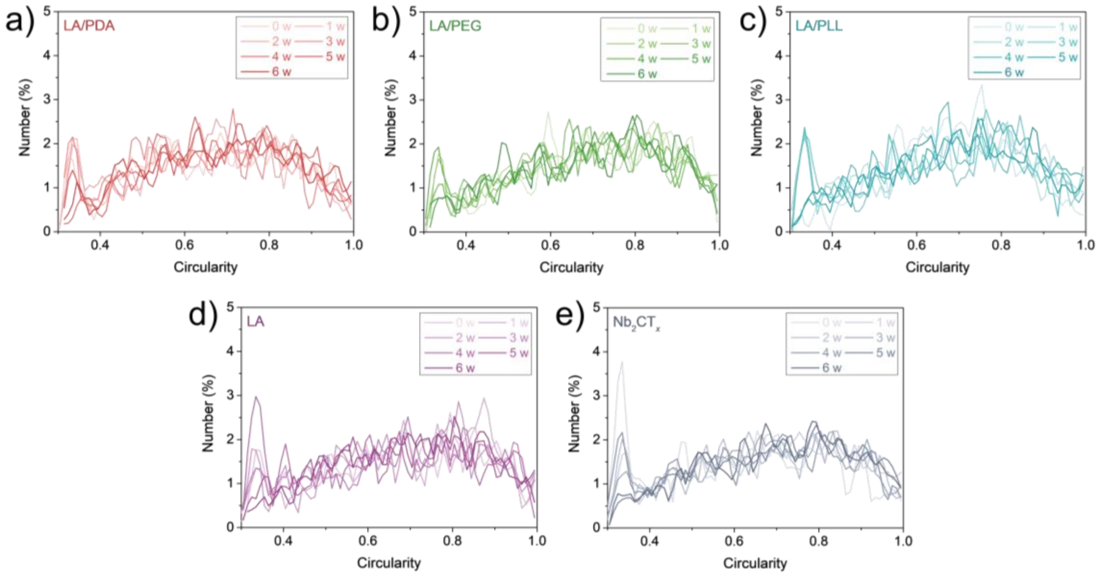

Fig. S7 Results of circularity coefficient measurements performed for the SL Nb_2CT_x MXene, stabilized with **(a)** LA/PDA, **(b)** LA/PEG, **(c)** LA/PLL, and **(d)** LA, as well as for **(e)** unmodified SL Nb_2CT_x MXene over time in PBS solution.

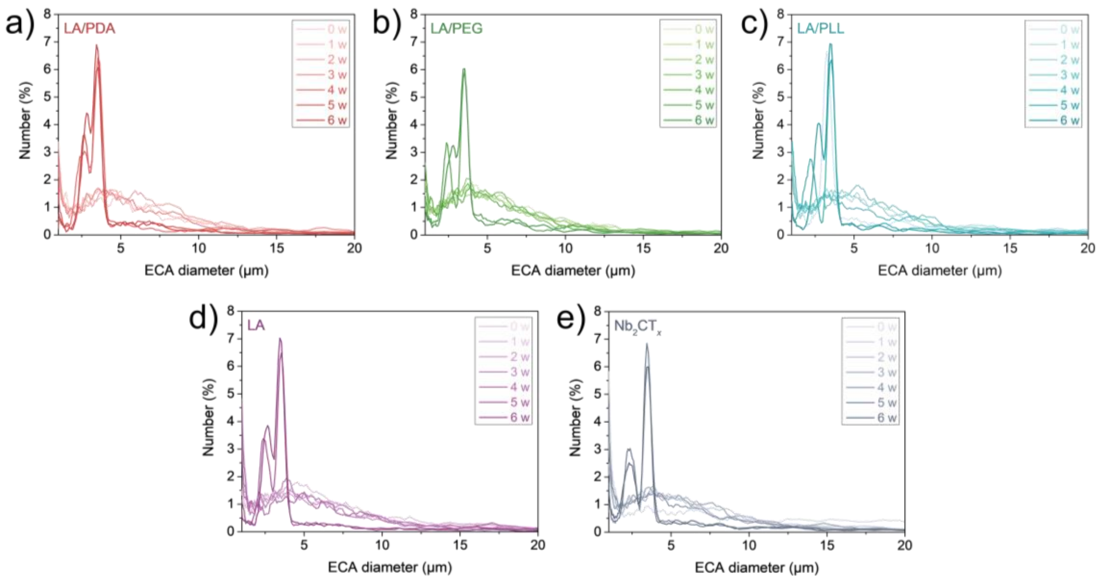

Fig. S8 Results of equivalent circular area diameter performed for the SL Nb_2CT_x MXene, stabilized with **(a)** LA/PDA, **(b)** LA/PEG, **(c)** LA/PLL, and **(d)** LA, as well as for **(e)** unmodified SL Nb_2CT_x MXene over time in the PBS solution.

References

[S1] Aydinyan S. Combustion synthesis of MAX phases: microstructure and properties inherited from the processing pathway. Crystals, 2023, 13(7): 1143

[S2] Salama I, El-Raghy T, Barsoum M W. Synthesis and mechanical properties of Nb_2AlC and $(Ti,Nb)_2AlC$. Journal of Alloys and Compounds, 2002, 347(1–2): 271–278

[S3] Dahlqvist M, Barsoum M W, Rosen J. MAX phases — past, present, and future. Materials Today, 2024, 72: 1–24